J. Fluid Mech. (2011), *vol.* 667, *pp.* 358–368.
doi:10.1017/S0022112010005641

The shape distribution of splash-form tektites predicted by numerical simulations of rotating fluid drops

S. L. BUTLER[1]†, M. R. STAUFFER[1], G. SINHA[1], A. LILLY[2] AND R. J. SPITERI[2]

[1]Department of Geological Sciences, University of Saskatchewan, Saskatoon Saskatchewan, S7N 5E2, Canada

[2]Department of Computer Science, University of Saskatchewan, Saskatoon Saskatchewan, S7N 5E2, Canada

(Received 22 July 2010; revised 20 October 2010; accepted 21 October 2010)

Splash-form tektites are glassy rocks ranging in size from roughly 1 to 100 mm that are believed to have formed from the splash of silicate liquid after a large terrestrial impact from which they are strewn over thousands of kilometres. They are found in an array of shapes including spheres, oblate ellipsoids, dumbbells, rods and possibly fragments of tori. It has recently become appreciated that surface tension and centrifugal forces associated with the rotation of fluid droplets are the main factors determining the shapes of these tektites. In this contribution, we compare the shape distribution of 1163 measured splash-form tektites with the results of the time evolution of a 3D numerical model of a rotating fluid drop with surface tension. We demonstrate that many aspects of the measured shape distribution can be explained by the results of the dynamical model.

Key words: drops, geophysical and geological flows, magma and lava flow

1. Introduction

Splash-form tektites are rocks that solidified from the splash of silicate material following a large Earth impact (Barnes & Barnes 1973; O'Keefe 1976; Koeberl 1994; Dressler & Reimold 2001; McCall 2001). The intriguing geometrical shapes in which they are found (Reinhart 1958) (see figure 1) have made them favourites of rock collectors. Elkins-Tanton *et al.* (2003) were the first to investigate the shapes of splash-form tektites in terms of the dynamics of rotating fluid drops, and they were able to produce many of the shapes of splash-form tektites in the laboratory using molten solder tumbling through air. They also showed, based on scaling arguments, that centrifugal and surface-tension forces should be dominant in determining the shapes of splash-form tektites. Only a few tektites show evidence of ground impact, such as plastic distortion or cracking of the outer portion, so it is generally believed that their shape quenches due to the increasing viscosity of the silicate melt as it cools in flight (Nininger & Huss 1967).

The first investigation of the shapes of rotating fluid drops was by Plateau (1863), who built an apparatus to rotate a fluid drop that was suspended with neutral

† Email address for correspondence: sam.butler@usask.ca

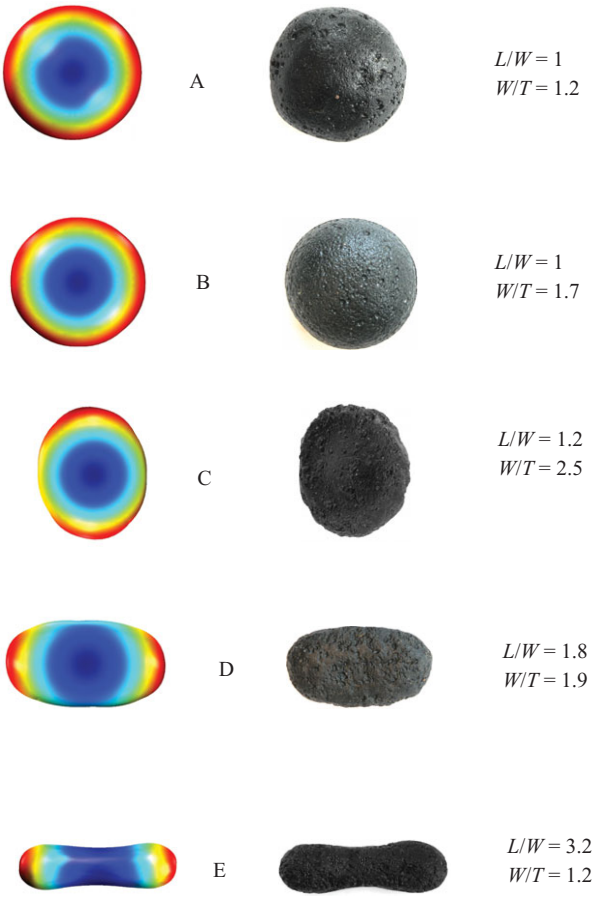

FIGURE 1. Left: snapshots of the outer surface of the numerical simulation with $L_a = 2.4$, $O_n = 1$ and $\delta = 0.01$. The view is looking down on the rotation axis. Colours indicate the square of the radial distance from the rotation axis ($x^2 + y^2$). Right: photographs of real tektites with similar axial ratios. Letters indicate shapes at the same times indicated in figures 2 and 4.

buoyancy in another immiscible fluid. He observed a myriad of shapes including ellipsoids, dumbbells and even a transient torus. Equilibrium shapes of rotating fluid drops that are symmetric about their rotation axis have been derived theoretically (Rayleigh 1914; Chandrasekhar 1965), and non-axisymmetric equilibrium shapes were later determined numerically (Brown & Scriven 1980; Heine 2006). It was also shown that if the dimensionless angular momentum of the drop is less than 1.2, where angular momentum is non-dimensionalized by the scaling $\sqrt{8\sigma\rho R^7}$, where σ, ρ and R are the surface tension coefficient, mass density and radius of a sphere of equivalent volume, stable axisymmetric oblate forms are obtained (see A and B in figure 1). If the scaled angular momentum is between 1.2 and 2.0, stable prolate or dumbbell shapes are found (see E in figure 1). When the scaled angular momentum is greater than 2.0, no stable shapes exist. Experimental microgravity space shuttle (Wang *et. al.* 1986, 1994) and magnetic levitation (Hill & Eaves 2008) studies have confirmed many of the predictions of the equilibrium theory. The forms of rotating fluid drops with surface tension have been a topic of significant theoretical and experimental

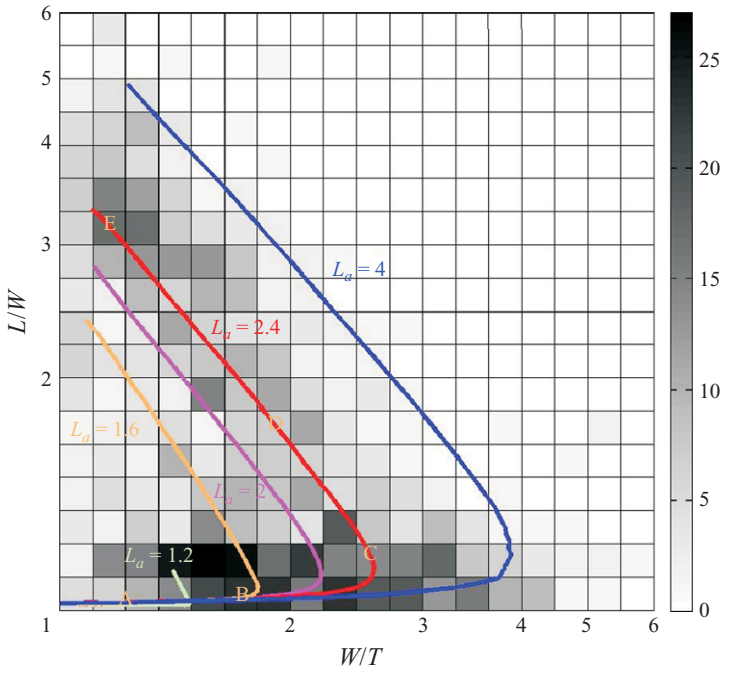

FIGURE 2. Greyscale, natural log, histogram of the number of tektites as a function of their axial ratios L/W and W/T. Coloured lines indicate the trajectory of 3D simulations with the angular momentum values: light green, 1.2; orange, 1.6; purple, 2; red, 2.4 and blue, 4; $O_n = 1$ and $\delta = 0.01$. Letters indicate the axial ratios for which snapshots are shown in figure 1.

interest, and they have been used as models for atomic nuclei (Bohr & Wheeler 1939), for self-gravitating astronomical objects, and even black holes (Cardoso & Gualtieri 2006).

In what follows, we first describe a database containing the dimensions of a large number of splash-form tektites. We then describe a numerical model of a deforming, rotating fluid drop with surface tension and, subsequently, we compare the distribution of shapes from the database with the shapes obtained from the numerical model.

2. A tektite database

A database was compiled by one of us (M.R.S.) that included the mass and the largest L, intermediate W and smallest T axis lengths of 1163 intact splash-form tektites found in Vietnam and Thailand that make up part of the 7.8×10^5-year-old Australasian tektite strewn field. The intermediate length was defined as the largest thickness perpendicular to the largest thickness axis, and the smallest thickness was defined as the greatest thickness perpendicular to both the longest and intermediate axes. In figure 2 we display a greyscale, 2D histogram of the number of tektites as a function of the ratios L/W and W/T. We refer to this type of diagram as a shape diagram. Such diagrams are commonly used to classify shapes in structural geology and are known as Flinn diagrams (Flinn 1962). For example, a sphere would be plotted at the origin of this diagram; an increasing distance from the origin indicates an increasing degree of deformation from spherical. Oblate ellipsoids plot near the horizontal axis, whereas prolate forms plot near the vertical axis. As can be seen, most of the tektites in the database are oblate, and the L/W and W/T ratios rarely exceed

4. It can also be seen that there are few weakly deformed, highly prolate tektites, which would correspond to short, stubby rods, and there appears to be a 'pathway' of increased tektite frequency connecting the oblate and prolate fields. Logarithmic axes were used for the histogram because L/W and W/T pairs calculated from randomly generated L, W and T triplets have a uniform angular distribution from the horizontal to the vertical axis.

Because only ratios are plotted, no information concerning the absolute size of tektites is conveyed in this figure. Additionally, because the largest thicknesses in perpendicular directions are measured, there is no distinction between tektites that show thinning near the rotation axis. For example, there is no distinction between rods and dumbbells or between ellipsoids and biconcave oblate shapes. A detailed analysis of the difference in shape distribution between large and small tektites and those that show central thinning and those that do not was carried out. Some small differences were noted and are discussed by Stauffer & Butler (2010).

The database of tektite lengths was compiled from measurements from tektite suppliers in Thailand and Vietnam. In total, 150 tektites were purchased in order to verify their measurements, and they were found to be reliable to within 1 mm. Tektite suppliers mine tektites for the purpose of selling them, and any sample larger than 20 g is picked up and measured. All mined tektites that became available over a one-year period were recorded ensuring a random sampling.

3. Numerical model

We solve the constant-viscosity, incompressible Navier–Stokes equations for fluid flow in a rotating reference frame that include a force-balance equation and a mass conservation equation:

$$\rho\left(\frac{\partial \boldsymbol{u}'}{\partial t'}+\boldsymbol{u}'\cdot\nabla'\boldsymbol{u}'\right)=-\nabla p'+\eta\nabla'^2\boldsymbol{u}+\rho\omega'^2\boldsymbol{r}'+2\rho\omega'\boldsymbol{u}'\times\hat{\boldsymbol{k}}+\rho\frac{\partial\omega'}{\partial t'}\boldsymbol{r}'\times\hat{\boldsymbol{k}}, \tag{3.1}$$

and

$$\nabla'\cdot\boldsymbol{u}'=0. \tag{3.2}$$

Here a prime indicates a dimensional variable. The dependent variables are $\boldsymbol{u}'$, which represents the fluid velocity, and p', which represents pressure. The term $\boldsymbol{r}'$ represents a radial vector from the rotation axis and t' represents time. The rotation axis is assumed to be fixed to the z-axis, and $\hat{\boldsymbol{k}}$ represents a unit vector in the z-direction and η represents the dynamic viscosity of the fluid. In (3.1), the terms on the right-hand side represent the pressure gradient, viscous, centrifugal, Coriolis, and Euler or Poincaré forces, respectively.

These equations are scaled for length, time and pressure by R, $\sqrt{\rho R^3 8^{-1}\sigma^{-1}}$ and $8\sigma R^{-1}$ to give the following dimensionless equations, where variables without primes are the dimensionless counterpart of those with primes:

$$\frac{\partial\boldsymbol{u}}{\partial t}+\boldsymbol{u}\cdot\nabla\boldsymbol{u}=-\nabla p+\frac{O_n}{2}\nabla^2\boldsymbol{u}+\omega^2\boldsymbol{r}+2\omega\boldsymbol{u}\times\hat{\boldsymbol{k}}+\frac{\partial\omega}{\partial t}\boldsymbol{r}\times\hat{\boldsymbol{k}} \tag{3.3}$$

and

$$\nabla\cdot\boldsymbol{u}=0. \tag{3.4}$$

The control parameters include the dimensionless angular momentum L_a, the Ohnesorge number $O_n=\eta(2\rho\sigma R)^{-0.5}$ and the initial length perturbation δ. The dimensionless time scale chosen here represents the deformation time for a fluid

drop deforming due to centrifugal forces with resisting surface tension, while O_n represents the ratio of time scales for deformation of a fluid with force balances between surface tension and viscosity, and surface tension and inertia.

As a drop deforms due to the centrifugal force, mass becomes distributed farther from the rotation axis, and the moment of inertia increases. The rotation rate ω was adjusted throughout each simulation so that the total angular momentum was constant.

The boundary conditions for the problem include a condition that the outer surface moves with the normal component of the velocity of the fluid. The tangential components of the stress on the outer boundary are required to be zero. Surface tension imparts a non-zero normal stress on the surface that is proportional to the curvature of the boundary and can be expressed as $\nabla_s \cdot \hat{\boldsymbol{n}}$, where $\hat{\boldsymbol{n}}$ is the unit normal to the droplet surface and $\nabla_s \cdot = (\boldsymbol{I} - \hat{\boldsymbol{n}}\hat{\boldsymbol{n}}^{\mathrm{T}})\nabla \cdot$ is the surface divergence. Here $\boldsymbol{I}$ represents the unit matrix in three dimensions and the superscript T represents the transpose operator.

When the force-balance equation is expressed in the weak form used with the finite element method, the curvature term times a velocity test function $\tilde{\boldsymbol{u}}$ is integrated by parts to give $\nabla_s \cdot \tilde{\boldsymbol{u}}/8$, which is set equal to the normal component of the stress times the velocity test function on the boundary (Walkley *et al.* 2005). The factor of 1/8 arises because of the non-dimensionalization of the equations.

The deforming boundary was modelled using the arbitrary Lagrangian–Eulerian technique that is built into the commercial finite-element modelling package Comsol. The model used 80 tetrahedral elements, and Winslow smoothing was used in order to specify the location of the internal mesh elements. When drops became highly deformed prolate shapes, it became necessary to remesh the solution at intervals during the calculation in order to maintain an adequate mesh quality.

The initial condition for the model was an ellipsoid, where one axis perpendicular to the rotation axis was of length $1+\delta$, and the other was of length $(1+\delta)^{-1}$, so that the volume was always $4\pi/3$, regardless of the size of the initial length perturbation.

As a check on the numerical model, we compare rotation rate versus angular momentum for steady states calculated from our numerical model (asterisks) plotted on top of the equilibrium theory results (Brown & Scriven 1980) (figure 3). Solid lines indicate stable equilibrium shapes, whereas dotted lines indicate unstable equilibrium shapes. Numerical model runs were carried out with $O_n = 1$, $\delta = 0.01$, and constant angular momentum. As angular momentum increases from zero, equilibrium theory predicts that the rotation rate initially increases linearly. At angular momenta where the drops deform significantly, the rate of increase of rotation rate with angular momentum decreases. At $L_a = 1.206$, there is a bifurcation point in the equilibrium curve where the descending branch represents the rotation rate for stable prolate shapes while the ascending branch represents unstable equilibrium oblate shapes. As can be seen, there is excellent agreement between the results of our transient simulations that were run to steady states and the equilibrium theory. The squares are data points taken from metastable oblate shapes that later became prolate during their transient evolution, and it can be seen that these are in excellent agreement with the rotation rates and angular momenta predicted for unstable equilibrium shapes. Note that the angular momentum given by Brown & Scriven (1980) is less by a factor of 4 from what we and Heine (2006) report. This discrepancy arises from the fact that Brown & Scriven (1980) did not properly account for the fact that they solved only a portion of the total drop and assumed equatorial and meridional symmetry (Heine 2003).

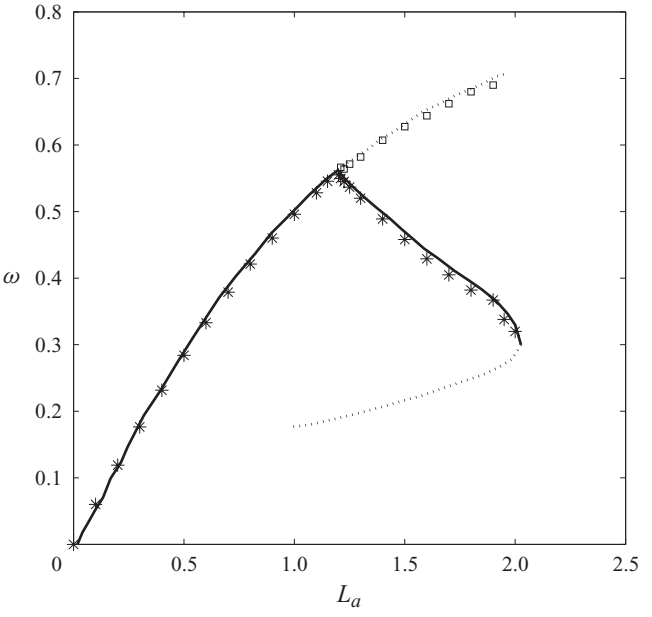

FIGURE 3. Angular momentum, L_a, versus rotation rate, ω, for equilibrium shapes. The lines indicate the results of equilibrium theory (solid line indicates stable equilibrium shapes, dotted line indicates unstable equilibrium shapes) while the asterisks are the results of our transient numerical model that was run to a steady state. The squares are results of our numerical model from transient unstable oblate shapes before they became prolate.

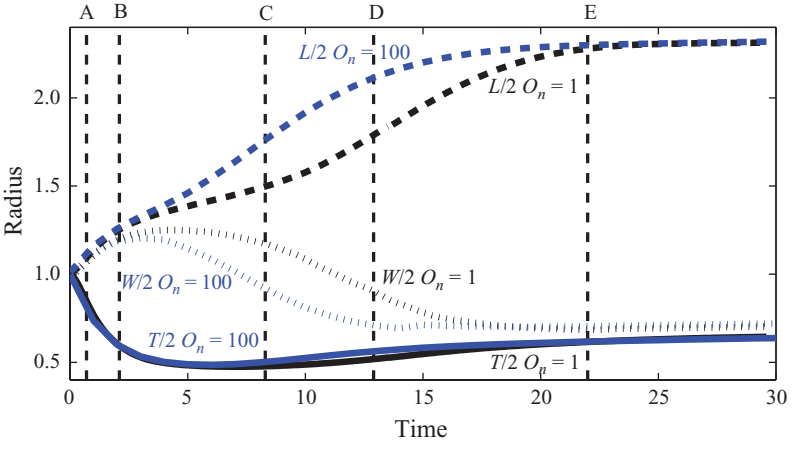

FIGURE 4. The time evolution of the largest, L, intermediate, W, and smallest, T, dimensions of a simulated fluid drop with $L_a = 2.4$ and $\delta = 0.01$, $O_n = 1$ (black) and $O_n = 100$ (blue). The time has been scaled by $1/100$ for the $O_n = 100$ results. Letters indicate the times for which snapshots are shown in figure 1.

4. Results

The time evolution of $L/2$, $W/2$ and $T/2$ is displayed in figure 4 for a simulation with $L_a = 2.4$, $O_n = 1$ and $\delta = 0.01$ (black lines). It can be seen that for dimensionless time from 3 to 8, $L/2$ and $W/2$ have similar dimensionless values near 1.3, while $T/2$ drops to roughly 0.5. During this time, the drop assumes an oblate shape. After

this time, the non-axisymmetric instability becomes significant; this is manifested by the increase in $L/2$ to 2.3, while $W/2$ decreases and $T/2$ increases to roughly 0.7 in time interval 8–20. Because $L_a > 2$, this drop will continue to deform and eventually pinch-off into two drops. This causes the slow variation of $L/2$, $W/2$ and $T/2$ at the end of the simulation. Our numerical scheme fails before pinch-off occurs. Similar blue lines are shown for a simulation with $O_n = 100$, the time scale for this case has been scaled by $1/100$. As can be seen, the time evolution is similar.

Using characteristic parameters for tektite materials of $\rho = 2500$ kg m^{-3}, $\sigma = 0.5$ N m^{-1}, and $R = 0.02$ m, one dimensionless time unit corresponds to roughly 0.07 s, meaning that the dimensional time in which the modelled tektites with $L_a = 2.4$ and $O_n = 1$ and $O_n = 100$ (figure 4) remained in the metastable oblate state were roughly 0.5 and 21 s, respectively, and the times to transition to a prolate form were roughly 0.5 and 70 s, respectively. The evolution time was seen to scale linearly with O_n for $O_n \gg 1$. The Ohnesorge number depends on the fluid viscosity, which is expected to change over many orders of magnitude as the fluid cools. Elkins-Tanton *et al.* (2003) estimated a range of O_n between 0.01 and 1000 for splash-form tektites.

Tektites cool on their surfaces by radiation and conduction to the air flowing over them, whereas their interiors cool by a combination of conduction, radiation and advection that results from the rotation-induced deformation. Assuming only conduction in the interior, an estimate of the characteristic cooling time, R^2/κ, gives a value of 400 s, where $\kappa = 10^{-6}$ m^2 s^{-1} (Eriksson, Hayashi & Seetharaman 2003) and $R = 0.02$ m. This is similar to the cooling time estimated by Klein, Yinnon & Uhlmann (1980), who also allowed for radiative heat transfer within the tektites. Clearly, the time needed for low-viscosity drops to deform is much shorter than the time needed to cool significantly. This indicates that low-viscosity tektites with $L_a > 2$ can be expected to have sufficient time to deform to pinch-off. The resulting new drops will also be rotating and may undergo another deformation evolution. The existence of transient, non-equilibrium shapes among tektites such as triaxial forms (e.g. D in figure 1) indicates that the time scales for deformation and cooling were similar for these tektites. The evolution and cooling times become similar when $O_n \sim 100$. Using the characteristic values as above, this implies a fluid viscosity of the order of 1000 Pa s, which is similar to the viscosity reported by Klein *et al.* (1980) for a tektite-derived liquid at 1300°C. The viscosity of molten tektites also depends on their silica concentration, which varies from one impact crater to another.

In figure 1, snapshots of the deforming exterior surface from the numerical simulation with $L_a = 2.4$, $O_n = 1$ and $\delta = 0.01$ are shown. The view is looking down from straight above the rotation axis, and the colour indicates the distance from the rotation axis. Also shown are photographs of splash-form tektites with similar axial ratios. Letters in figures 2 and 4 indicate the times at which the snapshots for figure 1 were taken. The evolution from a sphere to a flattened ellipsoid to a triaxial shape and then a dumbbell can be clearly seen. It can also be seen that the simulated fluid drop shapes bear a striking similarity to the shapes of real splash-form tektites. The transient shapes at A, B and E were compared with equilibrium shapes with similar axial ratios and were found to have very similar overall shapes. We were able to run models with $O_n > 0.1$ and $L_a < 5$. During the transient oblate phase, drops of all angular momenta and O_n with the same maximum radii had highly similar shapes.

A parametric curve of the simulated liquid fluid drop evolution with $L_a = 2.4$ is overlaid on the shape diagram in figure 2 (red line). The early evolution from a sphere to an oblate ellipsoid can be seen as the near-horizontal part along the x-axis. The curve bends sharply when the non-axisymmetric instability begins to significantly

affect the shape of the drop. It can also be seen that the parametric curve for $L_a = 2.4$, $O_n = 1$ and $\delta = 0.01$ follows the region of an increased tektite frequency reasonably well. A simulation with $L_a = 1.2$, $O_n = 1$ and $\delta = 0.01$ is also shown (green line). This simulated drop had an angular momentum that was just sufficient for the non-axisymmetric instability to occur. In this case, the drop evolved to a less-flattened ellipsoid than the drop with more angular momentum before undergoing the non-axisymmetric instability. Drops with angular momentum less than 1.2 did not undergo the non-axisymmetric instability and achieved a stable, equilibrium oblate shape with W/T less than 1.49. The orange, purple and blue lines show the results of simulations with $O_n = 1$, $\delta = 0.01$ and $L_a = 1.6$, 2 and 4, respectively.

In general, as the angular momentum increases, the drop evolves to an increasingly flattened oblate ellipsoidal shape before undergoing the non-axisymmetric instability. The resulting prolate drops are also increasingly flattened in the direction parallel to the rotation axis as angular momentum increases. As a result, because $L_a = 1.2$ is the lowest angular momentum for which the non-axisymmetric instability occurs, the model predicts that there should not be any drops in the roughly triangular area bounded by a horizontal line out to $W/T = 1.49$ and bounded to the right roughly by the orange curve. This can explain why there are few weakly deformed, prolate tektites. The fact that there are few intact tektites with W/T or L/W greater than 4 can be explained by the fact that stable equilibrium shapes do not exist for $L_a > 2$. If all tektites represented stable equilibrium shapes, then there would be no tektites on the right of the prolate branch of the purple curve. The tektites plotted on the right of this curve must represent shapes that solidified before pinch-off could occur. On the basis of scaling arguments, Elkins-Tanton *et al.* (2003) suggested that many tektites are likely to be unstable forms that quenched while in flight. Oblate tektites that are concave near the rotation axis and represent unstable equilibrium forms; their existence provides further support for this hypothesis. In figure 4, it can be seen that when $L_a = 2.4$, the drop attains a prolate shape that is close to stable and only slowly proceeds to pinch off. When L_a was increased significantly beyond 2, however, the drops seen were significantly flattened parallel to the rotation axis and did not attain an approximate equilibrium shape and continued to elongate. As a result, it becomes increasingly unlikely that solidification would occur before pinch-off as the angular momentum increases beyond 2, and the number of tektites with W/T or L/W greater than 4 may be expected to be few.

The fact that there is a large number of oblate tektites that are deformed with W/T greater than 1.49 indicates that these tektites quenched before the non-axisymmetric instability significantly affected their shape. The small number of triaxial tektites represent shapes that quenched during the transition from oblate to prolate.

Additional numerical simulations were carried out with other values of O_n and δ. In figure 5, we show the shape evolution for simulations with $L_a = 2.4$ with various values of O_n and δ. The red, purple and green lines indicate simulations with $\delta = 0.01$ and $O_n = 1$, 10 and 100. It can be seen that increasing O_n has the effect of rounding off the elbow in the curve but otherwise, the evolution of these simulations is quite similar. The yellow and orange lines represent simulations with $\delta = 0.05$ and $O_n = 1$ and 100. Increasing δ increases the 'prolateness' of the initial drop while increasing O_n rounds off the elbow in the curve. The simulations represented by the cyan and black lines had $\delta = 0.1$ and $O_n = 1$ and 100. A value for δ of at least 0.2 was necessary in order for the evolution curve through the shape diagram to pass through the region with decreased numbers of tektites in the highly prolate but weakly deformed field.

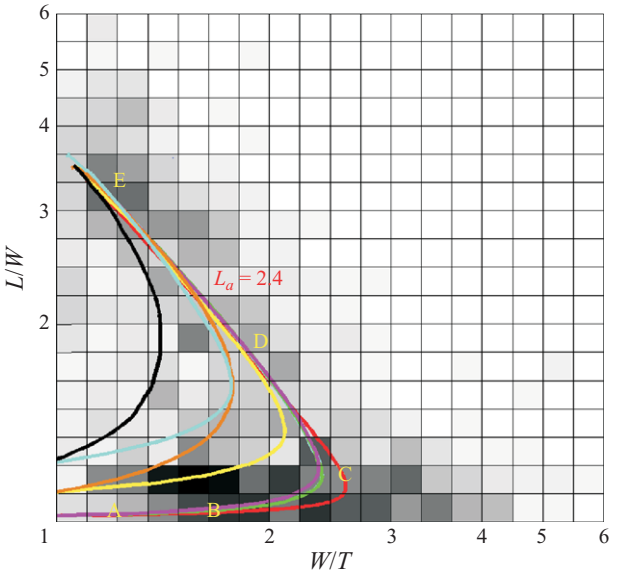

FIGURE 5. Greyscale, natural log, histogram of the number of tektites as a function of their axial ratios L/W and W/T for simulations with $L_a = 2.4$. Red, yellow and cyan lines show the shape trajectory for fluid drops with $O_n = 1$ and $\delta = 0.01$, 0.05 and 0.1. Purple, brown and black lines are from simulations with $O_n = 100$ and $\delta = 0.01$, 0.05 and 0.1, while the green line is from a simulation with $O_n = 10$ and $\delta = 0.01$.

5. Discussion and conclusions

We have shown that the shape distribution of intact splash-form tektites can be well explained by the time evolution of rotating fluid drops. The paucity of weakly deformed, prolate tektites can be explained by the fact that fluid drops first deform to oblate shapes before undergoing the non-axisymmetric instability to become prolate. The paucity of tektites with axial ratios greater than 4 can be explained by the fact that angular momenta greatly exceeding 2 are required to deform droplets to this degree, and hence such drops are expected to pinch-off before their shape can be quenched by cooling.

The deformation and cooling times of fluid drops are similar when $O_n \sim 100$. Transient, non-equilibrium shapes such as triaxial ellipsoids quenched while deforming, indicating that the characteristic deformation and cooling times must have been similar for these tektites, suggesting that $O_n \sim 100$ during their evolution. This value of O_n implies a viscosity on the order of 1000 Pa s, a value that is within the experimentally determined range of tektite material viscosities (Klein *et al.* 1980).

When O_n was less than 1, drops were observed to oscillate about equilibrium shapes when the angular momentum was sufficiently low that equilibrium shapes were seen. This raises the interesting possibility that some tektite shapes may have quenched while in mid-oscillation. The oscillations in our simulations, caused by the rotation-induced shape change, were all of fairly small amplitude. When the splash of silicate liquid following an Earth impact first breaks up into droplets, it is likely that there would be large perturbations that could induce large-amplitude oscillations. As a drop cools, its viscosity increases and we have shown that, at least in the late stages of evolution, the Ohnesorge number becomes much greater than 1. As a

result, oscillations are likely to be damped out and oscillations are not expected to significantly affect the distribution of tektite shapes.

The analyses of Brown & Scriven (1980) and Heine (2006) have shown that when $2 < L_a < 2.8$, there exist triangular unstable equilibrium shapes. In our transient simulations with this range of angular momenta, drops first became oblate and then became prolate and continued to stretch along their long axis until the numerical method fails. Triangular drops were not seen. It is possible that if we had initiated our simulations with a triangular perturbation, this shape might have evolved, but it appears that triangular shapes are sufficiently unstable that they are unlikely to occur during the transient evolution of liquid drops. Some very rare triangular tektites have been seen; however, their shapes may have been significantly modified by weathering processes on the ground.

One shortcoming of this analysis is that the viscosity of the modelled fluid drop is assumed to be constant. In real tektites, the viscosity increases as they cool, and it is this effect that quenches the final shape. If the tektite cools at roughly the same rate throughout its volume, then the effect is the same as increasing the Ohnesorge number with time; this was not found to significantly change the shape of the evolution curve on the shape diagram. It is likely, however, that the outside would cool faster than the inside, leading to higher viscosity on the outside than on the inside. This differential viscosity may affect the final shape of tektites. Also, the numerical calculation assumes no tangential stress on the outer boundary of the fluid drop, so that the effects of air friction are not taken into account. Furthermore, if lateral temperature variations exist on the outer surfaces of tektites, the surface tension coefficient would not be constant, and tangential stresses may result. Nonetheless, the similarity between the modelled fluid drops and real tektites is striking, and the fact that the main features of the tektite shape diagram can be explained by the results of our numerical model is highly suggestive.

REFERENCES

Barnes, V. E. & Barnes, M. A. 1973 *Tektites*. Dowden, Hutchinson and Ross Inc.

Bohr, N. & Wheeler, J. A. 1939 The mechanism of fission. *Phys. Rev.* **56**, 426–450.

Brown, R. A. & Scriven, L. E. 1980 The shape and stability of rotating liquid drops. *Proc. R. Soc. Lond.* A **371**, 331–357.

Cardoso, V. & Gualtieri, G. L. 2006 Equilibrium configurations of fluids and their stability in higher dimensions. *Class. Quant. Grav.* **23**, 7151–7198.

Chandrasekhar, S. 1965 The stability of a rotating liquid drop. *Proc. R. Soc. Lond.* A **286**, 1–26.

Dressler, B. O. & Reimold, W. U. 2001 Terrestrial impact melt rocks and glasses. *Earth-Sci. Rev.* **56**, 205–284.

Elkins-Tanton, L. T., Aussillous, P., Bico, J., Quéré, D. & Bush, J. W. M. 2003 A laboratory model of splash-form tektites. *Meteorit. Planet. Sci.* **38**, 1331–1340.

Eriksson, R., Hayashi, M. & Seetharaman, S. 2003 Thermal diffusivity measurements of silicate melts. *Intl J. Thermophys.* **24**, 785–797.

Flinn, D. 1962 On folding during three-dimensional progressive deformation. *Q. J. Geol. Soc.* **118**, 385.

Heine, C. 2006 Computations of form and stability of rotating drops with finite elements. *J. Numer. Anal.* **26**, 723–751.

Heine, C. 2003 Computations of form and stability of rotating drops with finite elements. PhD dissertation, Rheinisch-Westfalischen Technischen Hochschule Aachen, p. 101.

Hill, R. J. A. & Eaves, L. 2008 Nonaxisymmetric shapes of a magnetically levitated and spinning water droplet. *Phys. Rev. Lett.* **101**, 234501.

Klein, L. C., Yinnon, H. & Uhlmann, D. R. 1980 Viscous flow and crystallization behaviours of tektite glasses. *J. Geophys. Res.* **85**, 5485–5489.

Koeberl, C. 1994 Tektite origin by hypervelocity asteroidal or cometary impact: target rocks, source craters and mechanisms. *Geol. Soc. Am. Special Paper* **293**, 133–151.

McCall, J. 2001 *Tektites in the Geological Record: Showers of Glass from the Sky*. The Geological Society.

Nininger, H. H. & Huss, G. I. 1967 Tektites that were partially plastic after completion of surface sculpting. *Science* **157**, 61–62.

O'Keefe, J. A. 1976 *Tektites and Their Origin*. Elsevier.

Plateau, J. A. F. 1863 Experimental and theoretical researches on the figures of equilibrium of a liquid mass withdrawn from the action of gravity. *Annual Report of the Board of Regents of the Smithsonian Institution*, pp. 270–285. Washington, DC.

Rayleigh, Lord 1914 The equilibrium of revolving liquid under capillary force. *Phil. Mag.* **28**, 161–170.

Reinhart, J. S. 1958 Impact effects and tektites. *Geochim. Cosmochim. Acta* **14**, 287–290.

Stauffer, M. R. & Butler, S. L. 2010 The shapes of splash-form tektites: their geometrical analysis, classification and mechanics of formation. *Earth Moon Planet*. doi:10.1007/s11038-010-9359-y.

Walkley, M. A., Gaskell, P. H., Jimack, P. K., Kelmanson, M. A. & Summers, J. L. 2005 Finite element simulation of three-dimensional free-surface flow problems. *J. Sci. Comput.* **24**, 147–162.

Wang, T. G., Anilkumar, A. V., Lee, C. P. & Lin, K. C. 1994 Bifurcation of rotating liquid drops: results from USML-1 experiments in space. *J. Fluid Mech.* **276**, 389–403.

Wang, T. G., Trinh, E. H., Croonquist, A. P. & Elleman, D. D. 1986 Shapes of rotating free drops: spacelab experimental results. *Phys. Rev. Lett.* **56**, 452–455.